IS-T-661

THE SINGLE CRYSTALLINE ELASTIC CONSTANTS OF Al_2Cu AND Zr_2Ni

Frank Richard Eshelman

Ph. D. Thesis Submitted to Iowa State University

Ames Laboratory, ERDA
Iowa State University
Ames, Iowa 50010

MASTER

Date Transmitted: February 1975

PREPARED FOR THE U.S. ENERGY RESEARCH AND DEVELOPMENT ADMINISTRATION UNDER CONTRACT NO. W-7405-eng-82

NOTICE

This report was prepared as an account of work sponsored by the United States Government. Neither the United States nor the United States Energy Research and Development Administration, nor any of their employees, nor any of their contractors, subcontractors, or their employees, makes any warranty, express or implied, or assumes any legal liability or responsibility for the accuracy, completeness or usefulness of any information, apparatus, product or process disclosed, or represents that its use would not infringe privately owned rights.

DISTRIBUTION OF THIS DOCUMENT IS UNLIMITED

DISCLAIMER

This report was prepared as an account of work sponsored by an agency of the United States Government. Neither the United States Government nor any agency Thereof, nor any of their employees, makes any warranty, express or implied, or assumes any legal liability or responsibility for the accuracy, completeness, or usefulness of any information, apparatus, product, or process disclosed, or represents that its use would not infringe privately owned rights. Reference herein to any specific commercial product, process, or service by trade name, trademark, manufacturer, or otherwise does not necessarily constitute or imply its endorsement, recommendation, or favoring by the United States Government or any agency thereof. The views and opinions of authors expressed herein do not necessarily state or reflect those of the United States Government or any agency thereof.

DISCLAIMER

Portions of this document may be illegible in electronic image products. Images are produced from the best available original document.

NOTICE

This report was prepared as an account of work sponsored by the United States Government. Neither the United States nor the United States Energy Research and Development Administration, nor any of their employees, nor any of their contractors, subcontractors, or their employees, makes any warranty, express or implied, or assumes any legal liability or responsibility for the accuracy, completeness, or usefulness of any information, apparatus, product or process disclosed, or represents that its use would not infringe privately owned rights.

Available from: National Technical Information Service
U. S. Department of Commerce
P.O. Box 1553
Springfield, VA 22161

Price: Microfiche $2.25

TABLE OF CONTENTS

The single crystalline elastic constants of Al_2Cu and Zr_2Ni*

Frank Richard Eshelman

Under the supervision of J. F. Smith
From the Department of Metallurgy
Iowa State University

A pulse-echo-overlap system was used to measure the single crystalline elastic constants of the tetragonal Zr_2Ni and Al_2Cu phases in the temperature range 4.2 to 300 K. The mathematical relationships needed to calculate these elastic constants have been determined.

The longitudinal elastic constants of Zr_2Ni, C_{11} and C_{33}, both exhibit a monotonic decrease with increasing temperature. The C_{66} shear constant of Zr_2Ni has a 72% monotonic increase with increasing temperature in the 4.2 to 300 K temperature range and the other shear constants, C_{44} and $1/2(C_{11}-C_{12})$, are essentially temperature independent. The shear constants are noticeably smaller than the longitudinal constants, with C_{66} only 3.5% of C_{11} at 4.2 K.

All the elastic constants of Al_2Cu exhibit a monotonic decrease with increasing temperature. The C_{44} values of Al_2Cu show a 2% variation with direction that has been attributed to the presence of occluded particles of a second phase whose long dimension is oriented normal to the [001] direction.

---

*USAEC Report Is-T-661. This work was performed under contract W-7405-eng-82 with the Atomic Energy Commission.

There is evidence that Al_2Cu forms peritectically which gives rise to the second phase particles. Arguments are given to show that the maximum error from the occluded second phase particles is about 2%.

Zr_2Ni and Al_2Cu both have low longitudinal elastic anisotropy ratios and at least one high shear anisotropy ratio. In addition, one shear anisotropy ratio changes by 50% or more in the 4.2 to 300 K temperature range.

The polycrystalline moduli for Zr_2Ni and Al_2Cu from Voigt-Reuss-Hill averaging are given. The low shear modulus for Zr_2Ni is in keeping with the low values of the shear elastic constants of single crystals of this phase. The Debye temperatures for these phases are given.

INTRODUCTION

Single crystalline elastic constant measurements are an important means of gaining insight into the nature of intermetallic phases. Elasticity is closely associated with many of the physical, thermal, and mechanical properties. The intention of the present study is to examine the elastic properties of some compounds of the common Al_2Cu-type structures.

Al_2Cu is the prototype of the C16 "Strukturbericht" type (1). This structure has space group symmetry I4/mcm with point group symmetry 4/mmm. In these alloys, the Cu-type atoms are located at 0,0,1/4; 0,0,3/4; 1/2,1/2,1/4; and 1/2, 1/2,3/4 while the Al-type atoms are at 1/6,2/3,0; 5/6,1/3,0; 2/3,5/6,0; 1/3,1/6,0; 2/3,1/6,1/2; 1/3,5/6,1/2; 1/6,1/3,1/2; and 5/6,2/3,1/2. The Cu-type atoms thus form continuous chains parallel to the unique crystallographic axis while the Al-type atoms form a three-dimensional network separating the individual chains of the Cu-type species.

Crystal Elasticity

The equations of crystal elasticity can be derived from Hooke's law and Newton's second law of motion. Hooke's law states that in an elastic solid the stress is proportional to the strain. This is valid provided that the strain is sufficiently small. If higher order terms are neglected, the strain components can be defined by

$$e_{xx} = \frac{\partial u}{\partial x},\ e_{yy} = \frac{\partial v}{\partial y},\ e_{zz} = \frac{\partial w}{\partial z},\ e_{yz} = \frac{\partial v}{\partial z} + \frac{\partial w}{\partial y},$$
$$e_{zx} = \frac{\partial w}{\partial x} + \frac{\partial u}{\partial z},\ \text{and}\ e_{xy} = \frac{\partial u}{\partial y} + \frac{\partial v}{\partial x}\ , \tag{1}$$

where u, v, and w represent the displacements in the x, y, and z directions, respectively. Following the notation and development of Kittel (2), a capital letter designates the direction of force and the subscript the plane normal to which the force is applied. The stress components are X_x, X_y, X_z, Y_x, Y_y, Y_z, Z_x, Z_y, and Z_z. Since $Y_z = Z_y$, $Z_x = X_z$, and $X_y = Y_x$, the number of independent stress components reduces to six. These are X_x, Y_y, Z_z, Y_z, Z_x, and X_y. These notations allow us to write Hooke's law as six linear functions:

$$\begin{aligned}
X_x &= C_{11}e_{xx} + C_{12}e_{yy} + C_{13}e_{zz} + C_{14}e_{yz} + C_{15}e_{zx} + C_{16}e_{xy} \\
Y_y &= C_{21}e_{xx} + C_{22}e_{yy} + C_{23}e_{zz} + C_{24}e_{yz} + C_{25}e_{zx} + C_{26}e_{xy} \\
Z_z &= C_{31}e_{xx} + C_{32}e_{yy} + C_{33}e_{zz} + C_{34}e_{yz} + C_{35}e_{zx} + C_{36}e_{xy} \\
Y_z &= C_{41}e_{xx} + C_{42}e_{yy} + C_{43}e_{zz} + C_{44}e_{yz} + C_{45}e_{zx} + C_{46}e_{xy} \\
Z_x &= C_{51}e_{xx} + C_{52}e_{yy} + C_{53}e_{zz} + C_{54}e_{yz} + C_{55}e_{zx} + C_{56}e_{xy} \\
X_y &= C_{61}e_{xx} + C_{62}e_{yy} + C_{63}e_{zz} + C_{64}e_{yz} + C_{65}e_{zx} + C_{66}e_{xy}
\end{aligned} \tag{2}$$

The treatment in Kittel (2) shows that

$$C_{ij} = C_{ji}.$$

This reduces the number of constants in the above relationships to 21. Crystal symmetry further reduces this number to six for the 4/mmm Laue class of tetragonal crystals. The

elastic stiffness constant matrix thus becomes:

$$\begin{matrix} C_{11} & C_{12} & C_{13} & 0 & 0 & 0 \\ C_{12} & C_{11} & C_{13} & 0 & 0 & 0 \\ C_{13} & C_{13} & C_{33} & 0 & 0 & 0 \\ 0 & 0 & 0 & C_{44} & 0 & 0 \\ 0 & 0 & 0 & 0 & C_{44} & 0 \\ 0 & 0 & 0 & 0 & 0 & C_{66} \end{matrix} . \tag{3}$$

From Newton's second law of motion the following relations result:

$$\rho \frac{\partial^2 u}{\partial t^2} = \frac{\partial X_x}{\partial x} + \frac{\partial X_y}{\partial y} + \frac{\partial X_z}{\partial z}$$

$$\rho \frac{\partial^2 v}{\partial t^2} = \frac{\partial Y_x}{\partial x} + \frac{\partial Y_y}{\partial y} + \frac{\partial Y_z}{\partial z} = \frac{\partial X_y}{\partial x} + \frac{\partial Y_y}{\partial y} + \frac{\partial Y_z}{\partial z} \tag{4}$$

$$\rho \frac{\partial^2 w}{\partial t^2} = \frac{\partial Z_x}{\partial x} + \frac{\partial Z_y}{\partial y} + \frac{\partial Z_z}{\partial z} = \frac{\partial Z_x}{\partial x} + \frac{\partial Y_z}{\partial y} + \frac{\partial Z_z}{\partial z} .$$

Combining Equations 2 and 4 leads to:

$$\rho \frac{\partial^2 u}{\partial t^2} = C_{11}\frac{\partial e_{xx}}{\partial x} + C_{12}\frac{\partial e_{yy}}{\partial x} + C_{13}\frac{\partial e_{zz}}{\partial z} + C_{44}\frac{\partial e_{xz}}{\partial z} + C_{66}\frac{\partial e_{xy}}{\partial y}$$

$$\rho \frac{\partial^2 v}{\partial t^2} = C_{12}\frac{\partial e_{xx}}{\partial y} + C_{11}\frac{\partial e_{yy}}{\partial y} + C_{13}\frac{\partial e_{zz}}{\partial y} + C_{44}\frac{\partial e_{yz}}{\partial z} + C_{66}\frac{\partial e_{xy}}{\partial x} \tag{5}$$

$$\rho \frac{\partial^2 w}{\partial t^2} = C_{13}\frac{\partial e_{xx}}{\partial z} + C_{13}\frac{\partial e_{yy}}{\partial z} + C_{33}\frac{\partial e_{zz}}{\partial z} + C_{44}\frac{\partial e_{yz}}{\partial y} + C_{44}\frac{\partial e_{xz}}{\partial x} .$$

If the strain components defined in Equation 1 are substituted in these equations the following relationships are obtained:

$$\rho \frac{\partial^2 u}{\partial t^2} = C_{11}\frac{\partial^2 u}{\partial x^2} + C_{12}\frac{\partial^2 v}{\partial x \partial y} + C_{13}\frac{\partial^2 w}{\partial x \partial z} + C_{44}\left(\frac{\partial^2 w}{\partial x \partial z} + \frac{\partial^2 u}{\partial z^2}\right) + C_{66}\left(\frac{\partial^2 u}{\partial y^2} + \frac{\partial^2 y}{\partial x \partial y}\right) \tag{6a}$$

$$\rho \frac{\partial^2 v}{\partial t^2} = C_{12}\frac{\partial^2 u}{\partial x \partial y} + C_{11}\frac{\partial^2 v}{\partial y^2} + C_{13}\frac{\partial^2 w}{\partial y \partial z} + C_{44}\left(\frac{\partial^2 v}{\partial z^2} + \frac{\partial^2 w}{\partial y \partial z}\right) + C_{66}\left(\frac{\partial^2 u}{\partial y \partial x} + \frac{\partial^2 v}{\partial x^2}\right) \tag{6b}$$

$$\rho \frac{\partial^2 w}{\partial t^2} = C_{13}\left(\frac{\partial^2 u}{\partial x \partial z} + \frac{\partial^2 v}{\partial y \partial z}\right) + C_{33}\frac{\partial^2 w}{\partial z^2} + C_{44}\left(\frac{\partial^2 v}{\partial y \partial z} + \frac{\partial^2 w}{\partial y^2} + \frac{\partial^2 u}{\partial x \partial z} + \frac{\partial^2 w}{\partial x^2}\right). \tag{6c}$$

Table 1 lists the propagation directions and the polarization directions of the various plane waves together with the corresponding terms for ρV^2 for the 4/mmm class of tetragonal crystals. The development of these relations follows.

Waves propagated in the [100] direction

A longitudinal wave will have particle displacement that can be expressed by

$$u = u_o \exp[i(kx-\omega t)], \tag{7}$$

Table 1. The propagation directions and polarization directions of plane waves with the corresponding terms for ρV^2 for the 4/mmm class of tetragonal crystals

Propagation direction	Polarization direction	ρV^2
[100]	[100]	C_{11}
	[010]	C_{66}
	[001]	C_{44}
[001]	[001]	C_{33}
	[100] or [010]	C_{44}
[110]	[110]	$\frac{1}{2}(C_{11}+C_{12})+C_{66}$
	[1$\bar{1}$0]	$\frac{1}{2}(C_{11}-C_{12})$
	[001]	C_{44}
45° from [001] in (100)	45° from [001] in (100)	$\frac{1}{4}(C_{11}+C_{33}) + \frac{1}{2}C_{44} + \frac{1}{4}[(C_{11}-C_{33})^2+4(C_{13}+C_{44})^2]^{1/2}$
	45° from [001] in (010)	$\frac{1}{4}(C_{11}+C_{33}) + \frac{1}{2}C_{44} - \frac{1}{4}[C_{11}-C_{33})^2+4(C_{13}+C_{44})^2]^{1/2}$
	[100]	$\frac{1}{2}(C_{44}+C_{66})$

where u is the x component of the displacement, $k = 2\pi/\lambda$ is the wave vector with λ the wave length and $\omega = 2\pi\nu$ is the angular frequency. If Equation 7 is substituted into Equation 6a, the result is

$$\rho\omega^2 = C_{11}k^2. \tag{8}$$

The relationship between the velocity, V, the wavelength, λ, and the frequency, ν, is

$$V = \lambda\nu. \tag{9}$$

Introducing factors of 2π and substituting k and ω as defined above gives

$$V = \frac{\omega}{k}. \tag{10}$$

Substituting Equation 10 into Equation 8 results in

$$\rho V^2 = C_{11}. \tag{11}$$

A shear wave polarized in the [010] direction will have particle motion that can be represented by

$$v = v_o\exp[i(kx-\omega t)]. \tag{12}$$

Substituting this into Equation 6b gives

$$\rho\omega^2 = C_{66}k^2. \tag{13}$$

Combining this with Equation 10 as above results in

$$\rho V^2 = C_{66}. \tag{14}$$

In a similar manner a shear wave polarized in the [001] direction would give

$$w = w_o\exp[i(kx-\omega t)]. \tag{15}$$

Substituting this into Equation 6c gives

$$\rho\omega^2 = C_{44}k^2, \tag{16}$$

which reduces to

$$\rho V^2 = C_{44}. \tag{17}$$

Waves propagated in the [001] direction

A wave polarized longitudinally would have displacement

$$w = w_o \exp[i(kx-\omega t)]. \tag{18}$$

Combining this and Equation 6c gives

$$\rho\omega^2 = C_{33}k^2. \tag{19}$$

Substituting V into this results in

$$\rho V^2 = C_{33}. \tag{20}$$

A shear wave polarized in the [100] direction would have displacement

$$u = u_o \exp[i(kx-\omega t)]. \tag{21}$$

Combining this with Equation 6a gives

$$\rho\omega^2 = C_{44}k^2. \tag{22}$$

Substituting as above results in

$$\rho V^2 = C_{44}. \tag{23}$$

A wave polarized in the [010] direction produces displacement

$$v = v_o \exp[i(kx-\omega t)]. \tag{24}$$

When this is substituted into Equation 6b the result is

$$\rho\omega^2 = C_{44}k^2, \tag{25}$$

which reduces to

$$\rho V^2 = C_{44}. \tag{26}$$

Waves propagated in the [110] direction

The motion of a wave polarized in the [001] direction would be represented by

$$w = w_o \exp[i(k_x x + k_y y - \omega t)], \tag{27}$$

where $k_x = k_y = k(\cos 45°) = k/\sqrt{2}$.

If this is substituted into Equation 6c, the result is

$$\rho\omega^2 = C_{44}(k_x^2 + k_y^2) = C_{44}k^2 \tag{28}$$

and

$$\rho V^2 = C_{44}. \tag{29}$$

If waves are both propagated and polarized in the (110) plane, particle motion will be in both the x and y directions simultaneously, thus motion would be described by the two equations

$$u = u_o \exp[i(k_x x + k_y y - \omega t)] \tag{30}$$

and

$$v = v_o \exp[i(k_x x + k_y y - \omega t)], \tag{31}$$

where $k_x = k_y = k/\sqrt{2}$.

The results from these relationships and Equations 6a and 6b give

$$\rho\omega^2 u = (C_{11}k_x^2 + C_{66}k_y^2)u + (C_{12}k_x k_y + C_{66}k_x k_y)v \tag{32}$$

and

$$\rho\omega^2 v = (C_{12}k_xk_y+C_{66}k_xk_y)u + (C_{11}k_x^2+C_{66}k_y^2)v \qquad (33)$$

If substitutions are made for k_x and k_y, the results divided by k^2, and ω/k replaced by V, these equations can be rearranged to give

$$u[\tfrac{1}{2}(C_{11}+C_{66})-\rho V^2] + v[\tfrac{1}{2}(C_{12}+C_{66})] = 0 \qquad (34)$$

$$u[\tfrac{1}{2}(C_{12}+C_{66})] + v[\tfrac{1}{2}(C_{11}+C_{66})-\rho V^2] = 0 \qquad (35)$$

These will be satisfied if the determinant of the coefficients is zero. This gives a quadratic equation with two roots

$$\rho V^2 = \tfrac{1}{2}(C_{11}+C_{66}) \pm \tfrac{1}{2}(C_{12}+C_{66}) \qquad (36)$$

A longitudinal wave would then give

$$\rho V^2 = \tfrac{1}{2}(C_{11}+C_{12}) + C_{66} \qquad (37)$$

while a transverse wave polarized in $[1\bar{1}0]$ would give

$$\rho V^2 = \tfrac{1}{2}(C_{11}-C_{12}) \qquad (38)$$

Waves propagated in the (100) plane at an angle β to [001]

The particle motion for a wave polarized in the [100] direction would be represented by

$$u = u_o\exp[i(ky\ \sin\beta+kz\ \cos\beta-\omega t)]. \qquad (39)$$

Substituting as above into Equation 6a results in:

$$\rho\omega^2 = C_{44}k^2\cos^2\beta + C_{66}k^2\sin^2\beta. \qquad (40)$$

Substituting for ω^2 and k^2 gives:

$$\rho V^2 = C_{44}\cos^2\beta + C_{66}\sin^2\beta. \tag{41}$$

If $\beta = 45°$, then

$$\rho V^2 = \frac{1}{2}(C_{44}+C_{66}). \tag{42}$$

If a wave is propagated in the (100) plane at an angle of β to [001] and is also polarized in the (100) plane, particle motion would be in both the y and z directions. The equations of motion could then be described by

$$v = v_o\exp[i(ky\ \sin\beta+kz\ \cos\beta-\omega t)] \tag{43}$$

and

$$w = w_o\exp[i(ky\ \sin\beta+kz\ \cos\beta-\omega t)]. \tag{44}$$

Substituting these into Equations 6b and 6c gives

$$\rho\omega^2 v = (C_{11}k^2\sin^2\beta+C_{44}k^2\cos^2\beta)v + (C_{13}k^2\sin\beta\cos\beta + C_{44}k^2\sin\beta\cos\beta)w \tag{45}$$

and

$$\rho\omega^2 w = (C_{13}k^2\sin\beta\cos\beta+C_{44}k^2\sin\beta\cos\beta)v + (C_{33}k^2\cos^2\beta + C_{44}k^2\sin^2\beta)w. \tag{46}$$

Substituting $V^2 = \omega^2/k^2$ and rearranging Equations 45 and 46 results in:

$$(C_{11}\sin^2\beta+C_{44}\cos^2\beta-\rho V^2)v + (C_{13}\sin\beta\cos\beta+C_{44}\sin\beta\cos\beta)w = 0 \tag{47}$$

$$(C_{13}\sin\beta\cos\beta+C_{44}\sin\beta\cos\beta)v + (C_{33}\cos^2\beta+C_{44}\sin^2\beta-\rho V^2)w = 0. \tag{48}$$

These equations will be satisfied if the determinant of the coefficients vanishes. The result will be a quadratic equation in ρV^2 whose solutions are:

$$\rho V^2 = \frac{1}{2}(C_{11}\sin^2\beta+C_{33}\cos^2\beta+C_{44}) \pm \frac{1}{2}[(C_{11}\sin^2\beta-C_{33}\cos^2\beta)^2 + 4C_{13}^2\sin^2\beta\cos^2\beta+8C_{13}C_{44}\sin^2\beta+\cos^2\beta+C_{44} + 2C_{11}C_{44}\sin^2\beta\cos2\beta-2C_{33}C_{44}\cos^2\cos2\beta]^{1/2}. \quad (49)$$

If $\beta = 45°$ and the degree of anisotropy of thermal expansion is assumed to be negligibly small, this becomes:

$$\rho V^2 = \frac{1}{4}[C_{11}+C_{33}) + \frac{1}{2}C_{44} \pm \frac{1}{4}[(C_{11}-C_{33})^2 + 4(C_{13}+C_{44})^2]^{1/2}, \quad (50)$$

where the positive sign represents a longitudinally polarized wave and the negative sign a transversely polarized wave. Equation 50 can be simplified by subtraction. This gives

$$C_L - C_T = \frac{1}{2}[(C_{11}-C_{33})^2 + 4(C_{13}+C_{44})^2]^{1/2}, \quad (51)$$

where $C_L = V^2$ for the longitudinally polarized wave and $C_T = V^2$ for the transverse wave. Adding Equation 50 gives:

$$C_L + C_T = \frac{1}{2}(C_{11}+C_{33}) + C_{44}. \quad (52)$$

EXPERIMENTAL PROCEDURE

Sample Materials

All materials that were used in sample preparation were of high purity. Zirconium was obtained from Westinghouse Atomic Corp., and the supplier's analysis is given in Table 2. Belmont Smelting and Refining Works supplied the nickel and their analysis is also included in Table 2. The copper and aluminum were certified to be 99.999% pure and were supplied by Cominco American, Inc. and American Smelting and Refining Company, respectively. Again, the analyses as reported by the respective suppliers are given in Table 2.

Sample Preparation

The zirconium was made by the crystal-bar process, and the bars were ~3/4 inch in diameter. Lengths of these were etched in a mixture of 50% hydrofluoric acid and 50% nitric acid for about 2 minutes until the surface was bright. The bars were then cut into lengths about 3/4 inch long. Since the nickel that was used to make the alloys had a bright surface, no attempt was made to clean it. The copper was in the form of 1/4 inch bar stock. This was cut into lengths about 1/2 inch long and was surface cleaned for 2 minutes in a solution of 20% nitric acid. The aluminum was in the form of an ingot with a 2 inch square cross section. It was cut with a hack saw into cubes approximately 1/2 inch on an edge. Sur-

Table 2. Analyses of the metals used in preparing the alloys. Concentrations are listed in parts per million by weight

Impurity element	Zirconium	Nickel	Aluminum	Copper
C	43	100	-	-
Al	<35	-	-	-
Ti	42	-	-	-
Mn	<10	-	-	-
Fe	90	70	5	<0.7
Cu	-	10	2	-
S	-	20	-	<1
Sb	-	-	-	<1
Pb	-	-	-	<1
Sn	-	-	-	<1
Ni	-	-	-	<1
Bi	-	-	-	<0.1
Ag	-	-	-	<0.3
As	-	-	-	<2
Cr	-	-	-	<0.5
Si	-	-	-	<0.1
Te	-	-	-	<2
Se	-	-	-	<1
N	<5	-	-	-

face irregularities were removed by hand filing and the cubes were then etched in a solution of sodium hydroxide for about 5 minutes.

Stoichiometric weights corresponding to the composition of the desired phase were arc melted under an inert atmosphere using a non-consumable tungsten electrode with the procedure described by Hungsberg and Gschneidner (3). Homogeneity was facilitated by repeated arc melting with the solidified sample being inverted between each successive melting.

The Zr_2Ni alloys were sealed under argon in 0.75 inch diameter tungsten crucibles having conical tips. The crystals were then grown in a Bridgman furnace under pressures of 10^{-5} Torr or less. Zr_2Ni did not adhere to the crucibles and was removed by cutting the tops off the crucibles and sliding the samples out.

The Al_2Cu crystals were grown in 0.75 inch tantalum crucibles in a manner similar to that used in preparing the Zr_2Ni samples. Al_2Cu shatters easily and the crucibles were cut away from the samples using an electrospark cutting machine. No perfect crystals of Al_2Cu were produced. Figures 1(a) and 1(b) are photomicrographs of the (001) and (100) faces, respectively, of these crystals showing the size and extent of an occluded second phase. The effect of this second phase will be discussed in a later section.

To facilitate alignment and cutting, the crystals were

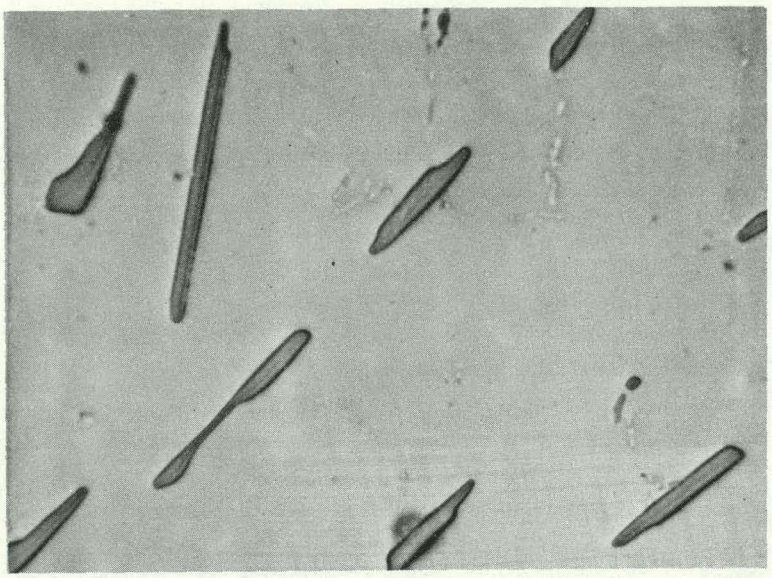

(a)

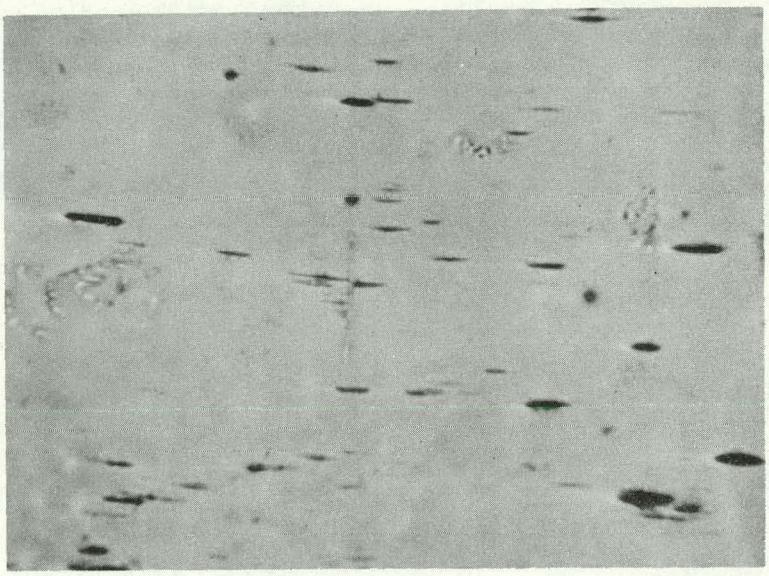

(b)

Figure 1. Photomicrographs of Al_2Cu (200X). (a) is the (001) face and (b) is the (100) face with [001] vertical

attached to a goniometer head with an electrically conducting mixture of Duco cement and graphite powder. The Zr_2Ni crystals were further electrically grounded by attaching a copper wire to the goniometer base and affixing the opposite end of the wire to the crystal with electrically conducting silver cement. Grounding the Al_2Cu crystals with a wire was not found to be necessary. The desired crystallographic direction was located by means of X-ray diffraction with the back reflection technique of Meyerhoff, Bailey, and Smith (4). The goniometer with the crystal in place was then transferred to a Sparcatron electrospark cutting machine. Three crystals were machined with faces normal to the [100], [110], and the [001] crystallographic axis, respectively. A fourth crystal was cut with faces parallel to the [010] axis and at an angle of 45° to both the [100] and the [001] axis. The faces of the samples were hand-lapped on progressively finer metallographic polishing paper, finishing with 600 grit paper. The samples were then rechecked with X-rays using the back reflection Laue method to insure that they were properly aligned and that there was no evidence of worked metal.

Instrumentation

The pulse-echo-overlap method was used to measure the transit times of the individual crystals. The overlap technique is one of several ultrasonic pulse-echo methods. May (5) and Papadakis (6) developed the method and it was later

modified by Chung, Silversmith, and Chick (7). The electronic instrumentation that was used in this investigation represents a simplification of the earlier overlap systems. The pulse-echo-overlap method has several advantages over other ultrasonic pulse-echo methods. It allows cycle by cycle examination of the echoes which can essentially eliminate any ambiguity in the proper matching of the echo envelopes. Another advantage is that a transit time datum can be taken in a few seconds which facilitates measuring the transit time at relatively short temperature intervals. A further advantage of the system is that the matching of successive echoes permits reproducibility to within about 0.05% for most time measurements and permits measurements on samples whose delay times are only slightly greater than the pulse length. In addition, since only two distinct echoes are needed, measurements can be made on samples that are highly attenuating.

A block diagram of the pulse-echo-overlap apparatus is shown in Figure 2. The counter, pulse generator, and oscilloscope are Hewlett-Packard units 5325B, 222A, and 180 with 1801A and 1820A plug-in units, respectively. The repetition-rate generator is a Waveform 402A audio generator and the pulsed oscillator is an Arenberg model PG-650C. The frequency divider and limiter were constructed especially for this instrumentation. The frequency divider circuit is shown in Figure 3. Three Fairchild CμL9958 decade counters form the

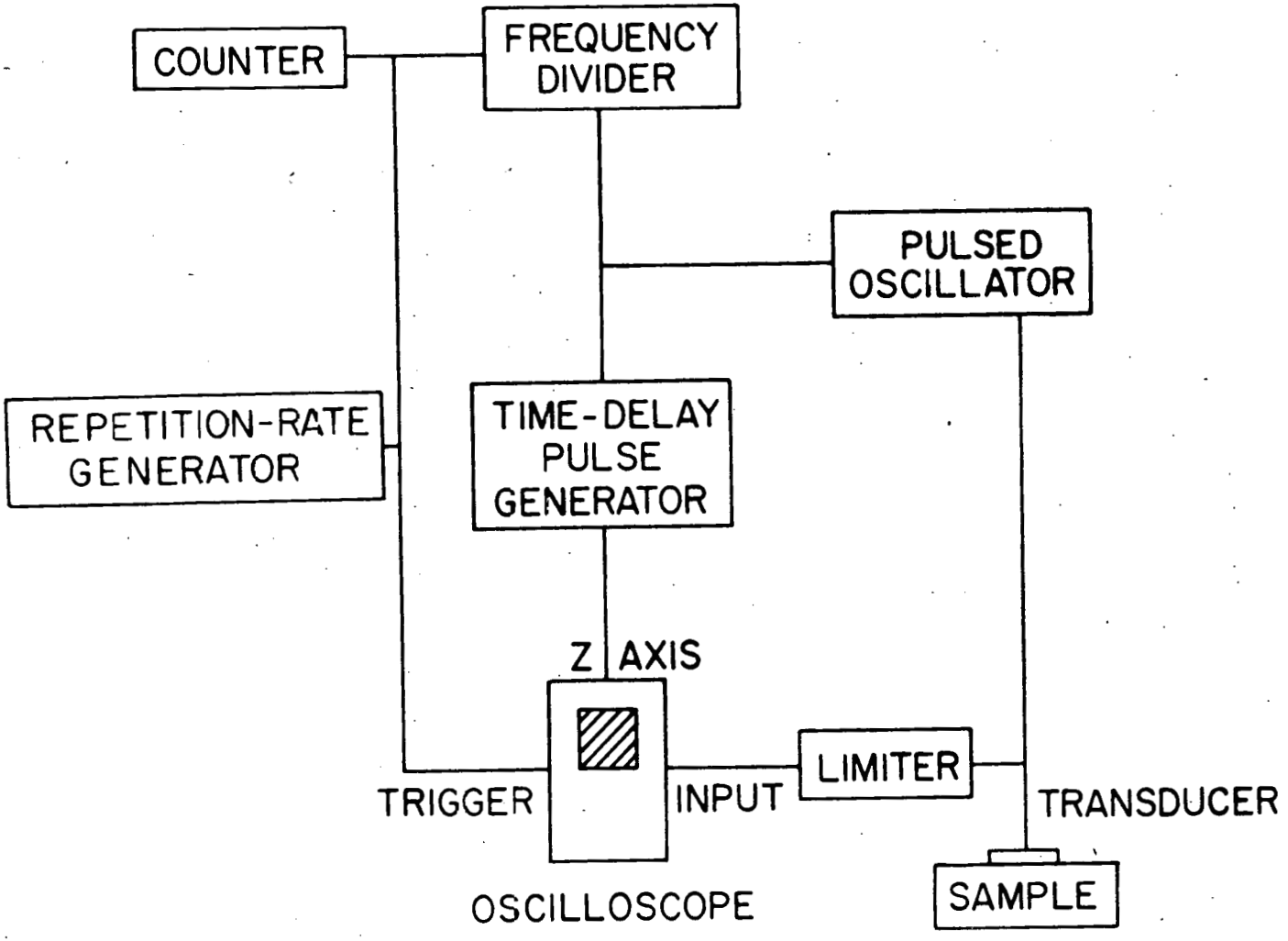

Figure 2. Block diagram of the pulse-echo-overlap apparatus

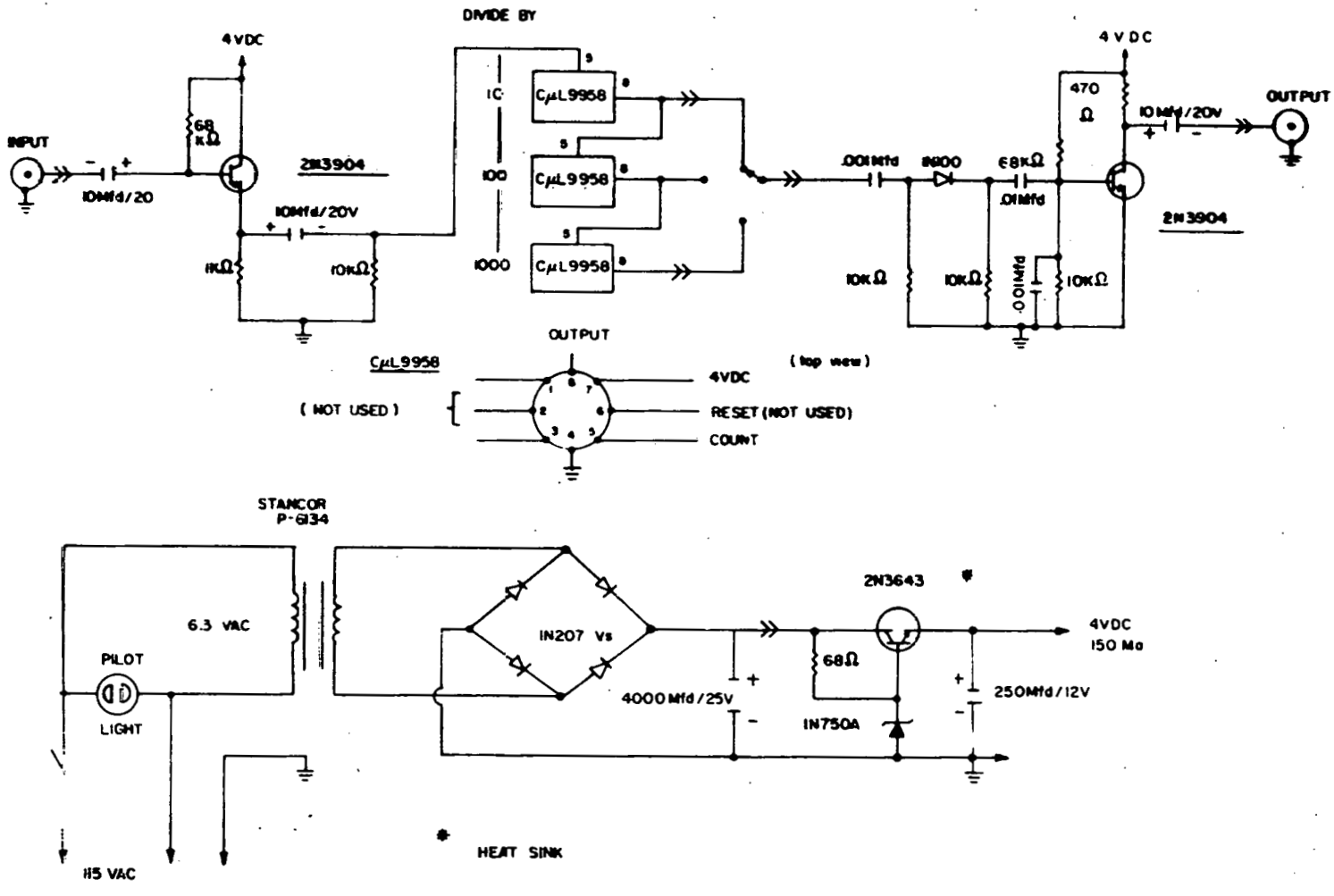

Figure 3. Schematic diagram of the frequency divider

heart of the divider. A switch allows the unit to be set for division by 10, 100, or 1000 and a one-transistor output provides a 4 volt negative spike which triggers the pulse generator and the pulsed oscillator. The limiter circuit is shown in Figure 4. Two 1N914 diodes are wired in parallel with opposite polarity. These are conductive above a few volts but are non-conductive for small voltages. The limiter clips the high voltage pulse from the pulsed oscillator while reducing the echo amplitude by only about 10%. This prevents overloading the oscilloscope and allows the use of higher pulse voltages.

Use of the Pulse-Echo-Overlap System

In using the system, the pulse generator amplitude is initially turned down and the oscilloscope triggered internally. The repetition-rate generator is adjusted to a convenient period (5 microseconds) and the oscilloscope adjusted to allow observation of the echo train. The approximate transit time can then be observed on the oscilloscope screen. Next the repetition-rate generator is adjusted to this period and the oscilloscope intensity turned down. The echoes selected for observation are displayed by increasing the pulse generator amplitude and adjusting the pulse delay and pulse length. At this stage the system is ready to be switched to the pulse-echo-overlap mode.

The oscilloscope triggered switch is moved to the external

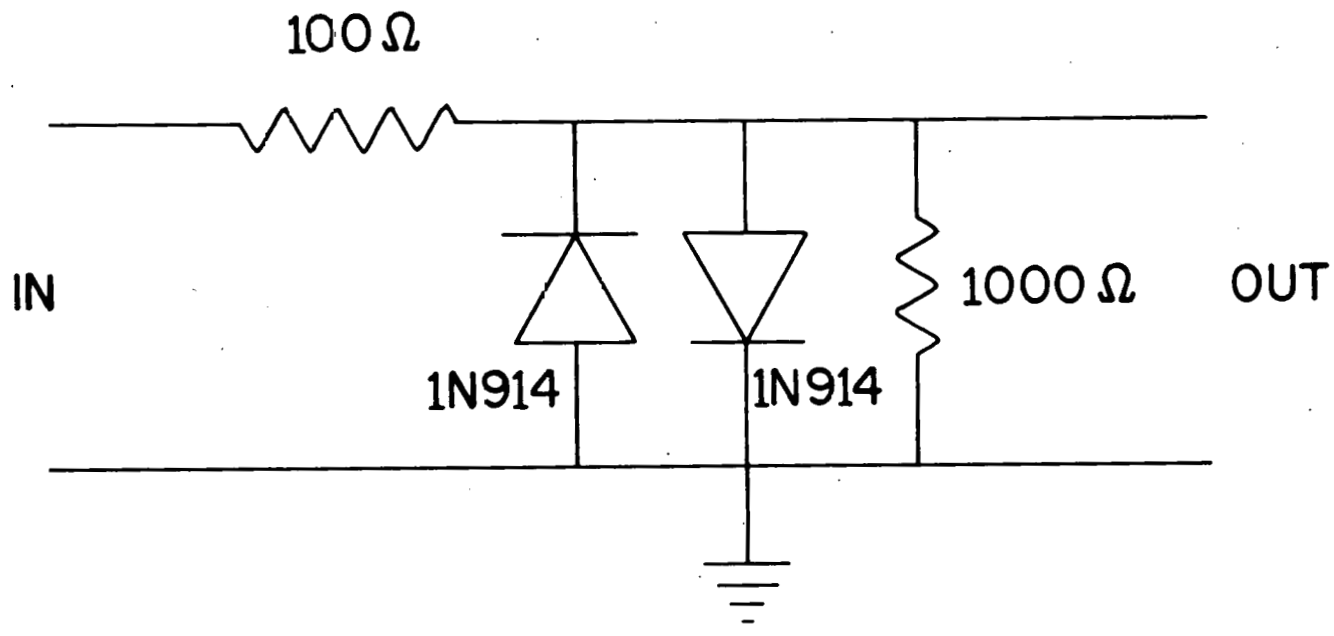

Figure 4. Schematic diagram of the limiter

position so that the repetition-rate generator triggers the oscilloscope. Adjustments are made in the frequency of the repetition-rate generator to cause the second echo to superimpose upon the first. Reading the period of the repetition-rate oscillator gives a direct measure of the transit time.

Wave Velocity Determination

The individual elastic constants were determined from the respective plane velocities. The velocities were calculated from the transit times using the relationship

$$V = \frac{2d}{t} \tag{52}$$

where V is the wave velocity, d the thickness of the crystal under examination, and t the time required for the wave to travel from one face to the opposite face and return to the first face.

A micrometer giving direct readings to 0.0001 inch was used to make room temperature measurements of the sample thickness. Three measurements were taken on each face, and the micrometer was moved between each reading. The three measurements for each face agreed within the precision of the micrometer.

Sample temperatures were determined with thermocouples taped to the crystals. A Au + 0.03 a/o Fe vs Ag thermocouple was used over the temperature range 4.2 to 50 K and a copper vs constantan thermocouple was used in the 40 to 300 K tem-

perature range.

The longitudinal and transverse waves were generated by X and Y-cut quartz transducers having resonance frequencies of 10 MHz. The bonding agent for all measurements using X-cut transducers was Nonaq stopcock grease. The Y-cut transducers were bonded to the samples with Nonaq stopcock grease for data taken at temperatures below 270 K and with salol (phenyl salicylate) for measurements over the 250 to 300 K temperature range.

The crystal under examination was mounted in a copper sample holder. At low temperatures, when Nonaq was used as the bonding agent, the data were taken with the sample holder suspended in a cryostat consisting of two concentric Dewars. Figure 5 is a cross-sectional illustration of the cryostat with the sample holder and sample in place. Over the temperature range 77 to 300 K liquid nitrogen was maintained in the outer Dewar. Pressure in the vacuum chamber of the inner Dewar was varied to control thermal conductivity and hence the cooling rate of the sample. The transit time data were taken as the sample cooled over a period of several hours. For transit time measurements at temperatures below 77 K, it was necessary to refrigerate with liquid helium. A mechanical pump was used to produce a vacuum of at least 10 microns in the vacuum chamber of the inner Dewar and then sufficient liquid helium was transferred into the cryostat to immerse

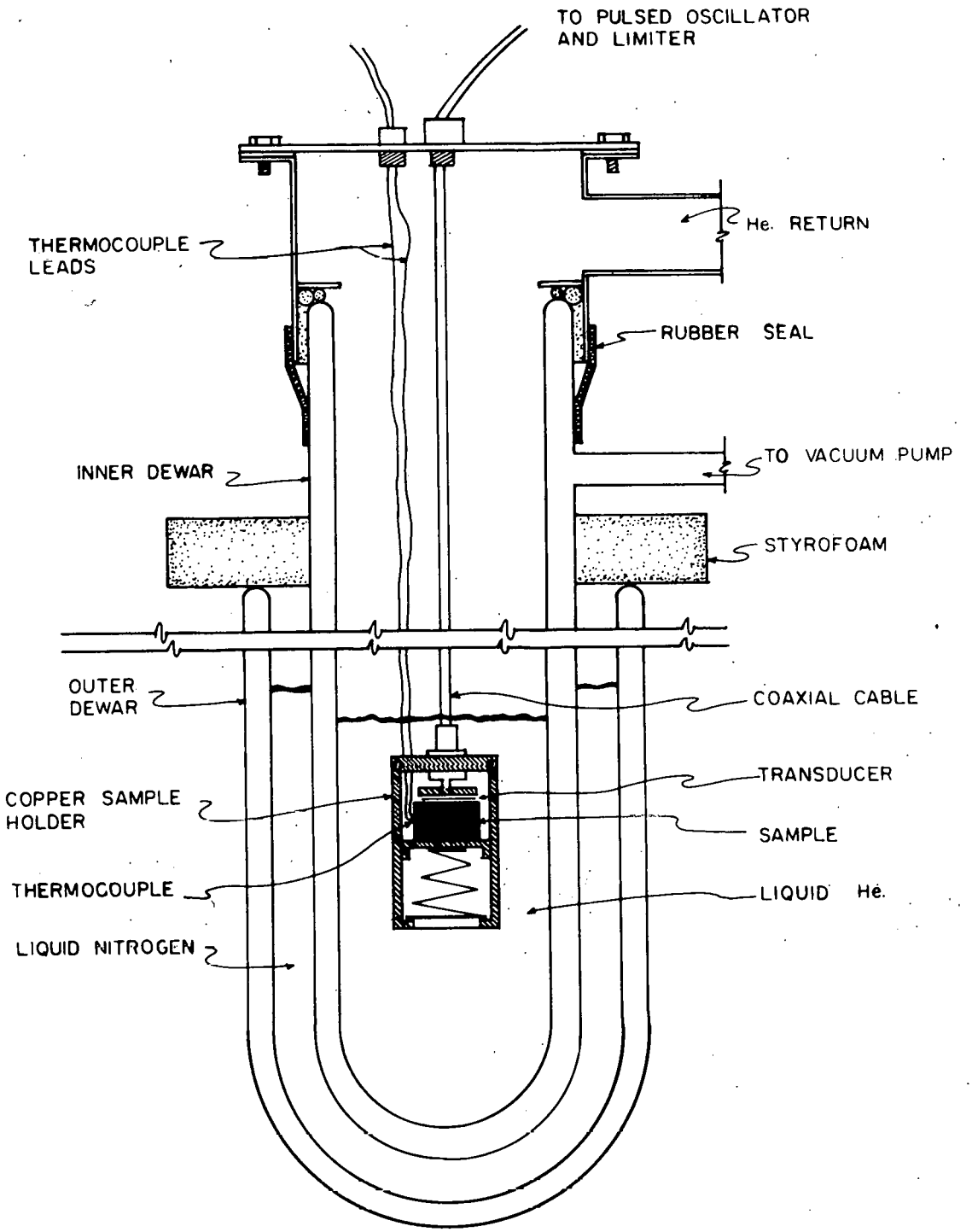

Figure 5. Cross section of cryostat with sample holder and sample in place

the sample holder and the sample. The transit time at 4.2 K was then taken. Transit time data in the temperature range 4.2 to 77 K were taken as the liquid helium slowly boiled away and the sample warmed toward liquid nitrogen temperature. Since the temperature changes were not rapid and the samples were mounted in a copper sample holder, temperature gradients were small and the associated errors negligible.

When salol was used as the bonding agent, a different sample holder was used and this sample holder was mounted in a closely fitting heat sink which minimized temperature gradients. Transit time measurements in the 250 to 300 K temperature range were made by suspending the sample holder assembly in a Dewar above boiling liquid nitrogen.

RESULTS

The directly measured quantities were the transit times. These transit times were converted to wave velocities via Equation 52 and these velocities were then converted to elastic constants with the ρV^2 relationships of Table 1. This gave the raw elastic constant data for C_{11}, C_{33}, C_{44}, C_{66}, $1/2(C_{11}-C_{12})$, C_L, and C_T. Values for these constants as functions of temperature for Zr_2Ni are shown in Figures 6 and 7 and for Al_2Cu in Figures 8 and 9. The third law of thermodynamics requires a zero slope at 0 K for curves of elastic constant vs temperature and the figures were drawn accordingly. Smoothed values from interpolated curves for these constants and calculated values for C_{12} and C_{13} are given in Table 3 for Zr_2Ni and in Table 4 for Al_2Cu. In the foregoing treatment density and dimensional changes have been neglected because no data covering thermal expansion are available.

The calculation of C_{13} requires the extraction of a square root with an attendant sign ambiguity. Alers and Neighbours (8) have discussed the resolution of this sign ambiguity in terms of crystal stability and have given the mathematical requirements relating the elastic constants to crystal stability. In the case of Zr_2Ni only the positive root satisfies these requirements. However, in the case of Al_2Cu both roots satisfy the stability requirements and the selection of the correct value was made by other means.

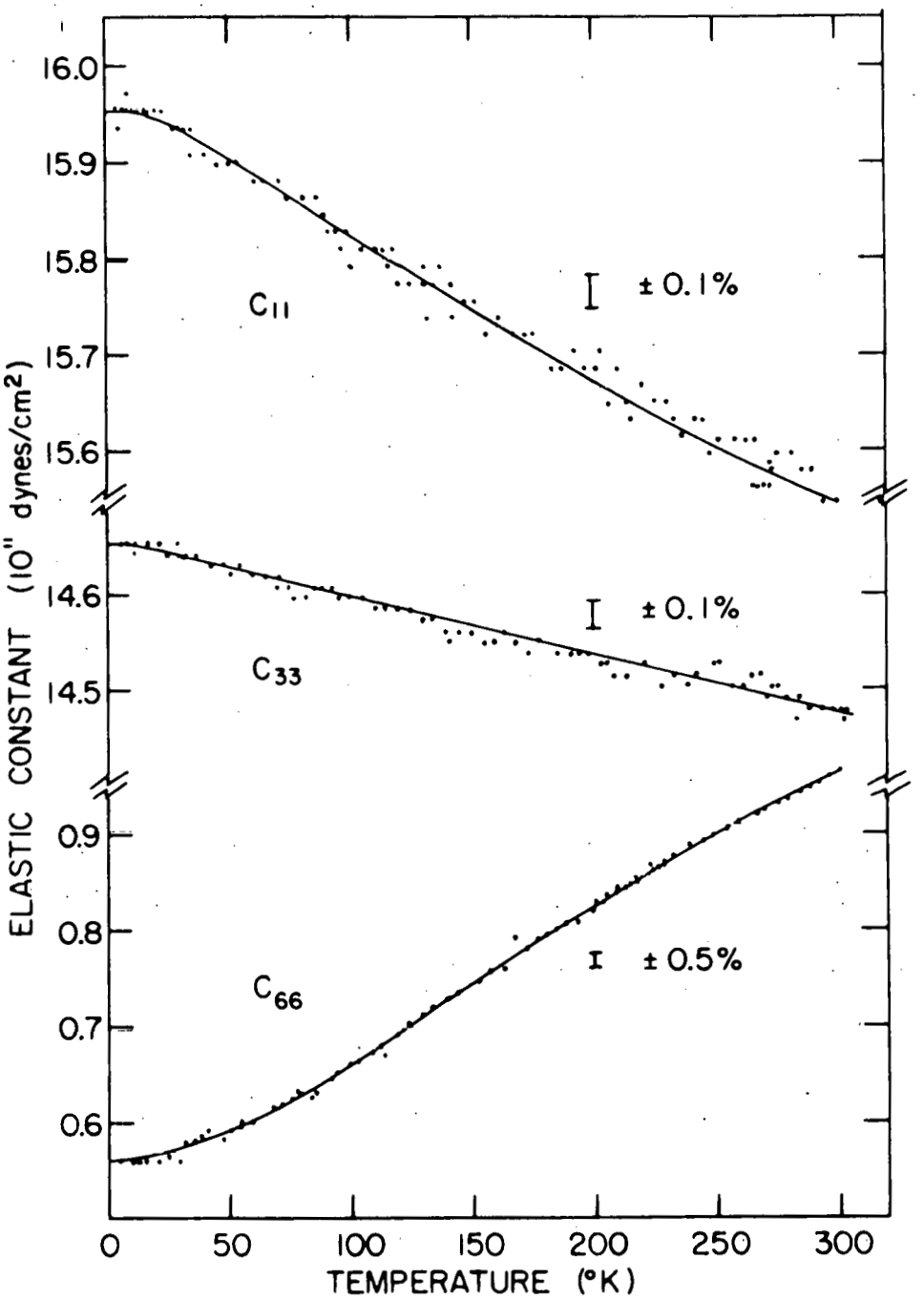

Figure 6. Single crystalline elastic constant data for Zr_2Ni

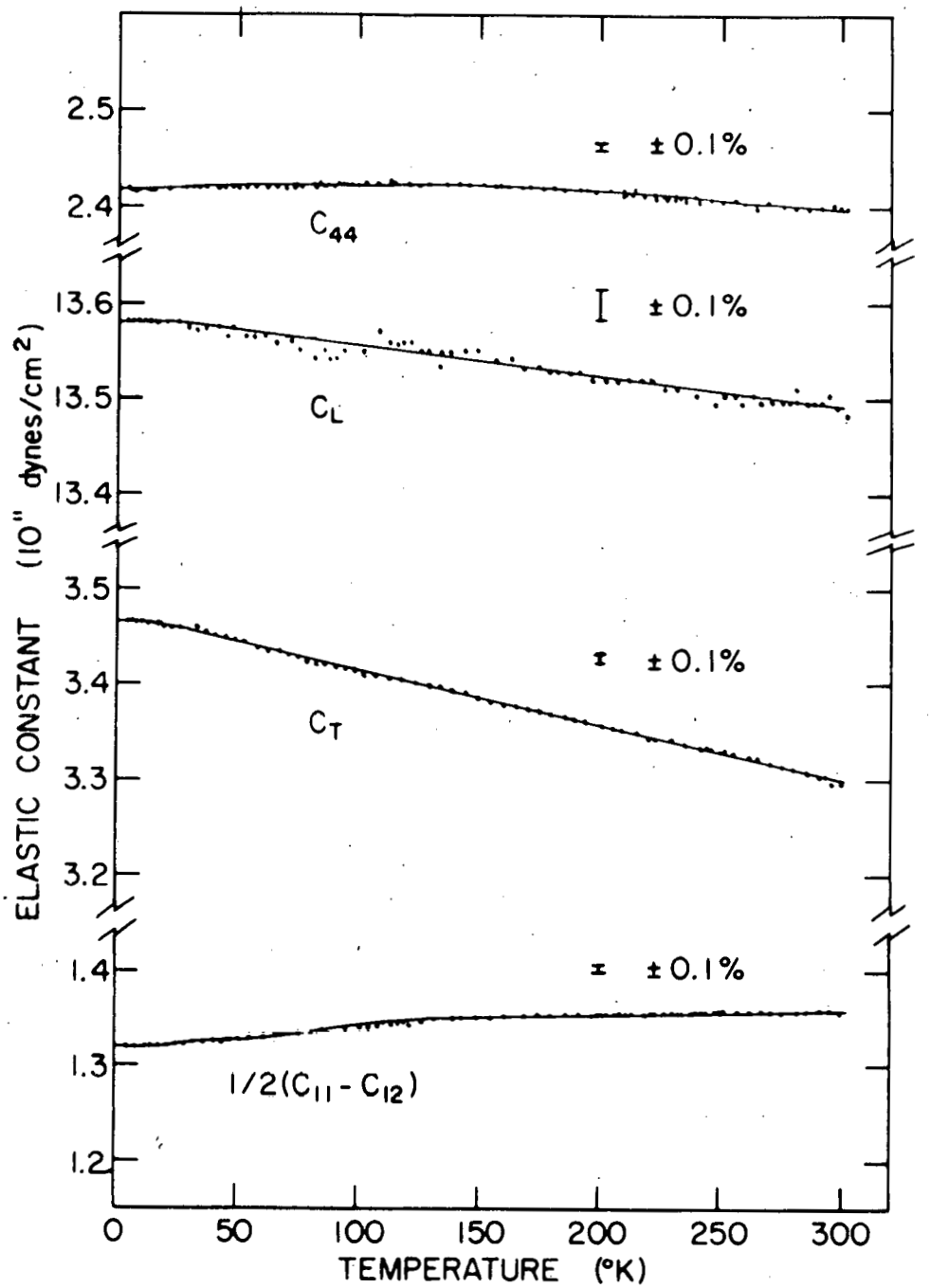

Figure 7. Single crystalline elastic constant data for Zr_2Ni. C_L and C_T are associated with the quasi-longitudinal and quasi-transverse waves, respectively, propagated at 45° to [001] in (100)

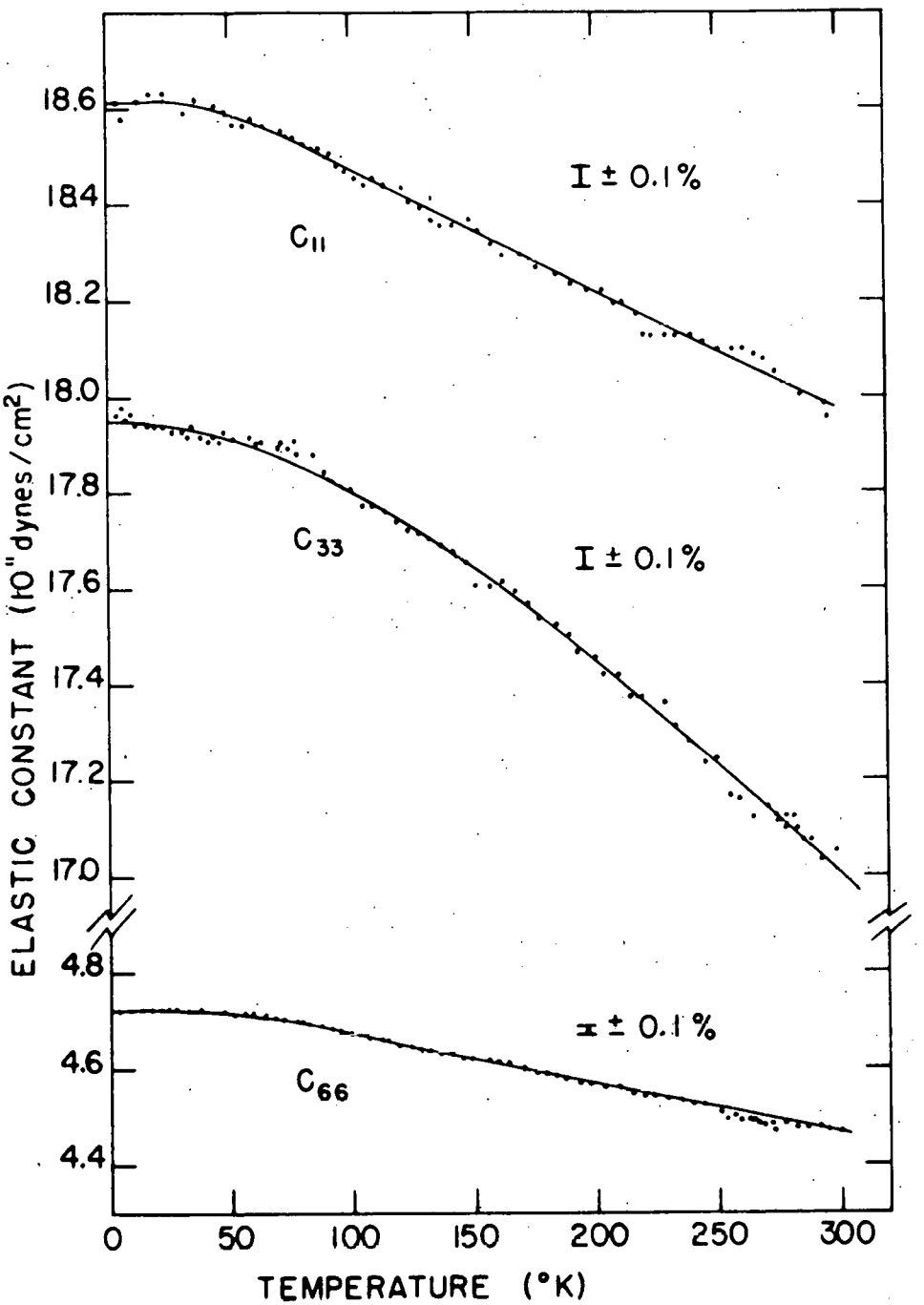

Figure 8. Single crystalline elastic constant date for Al_2Cu

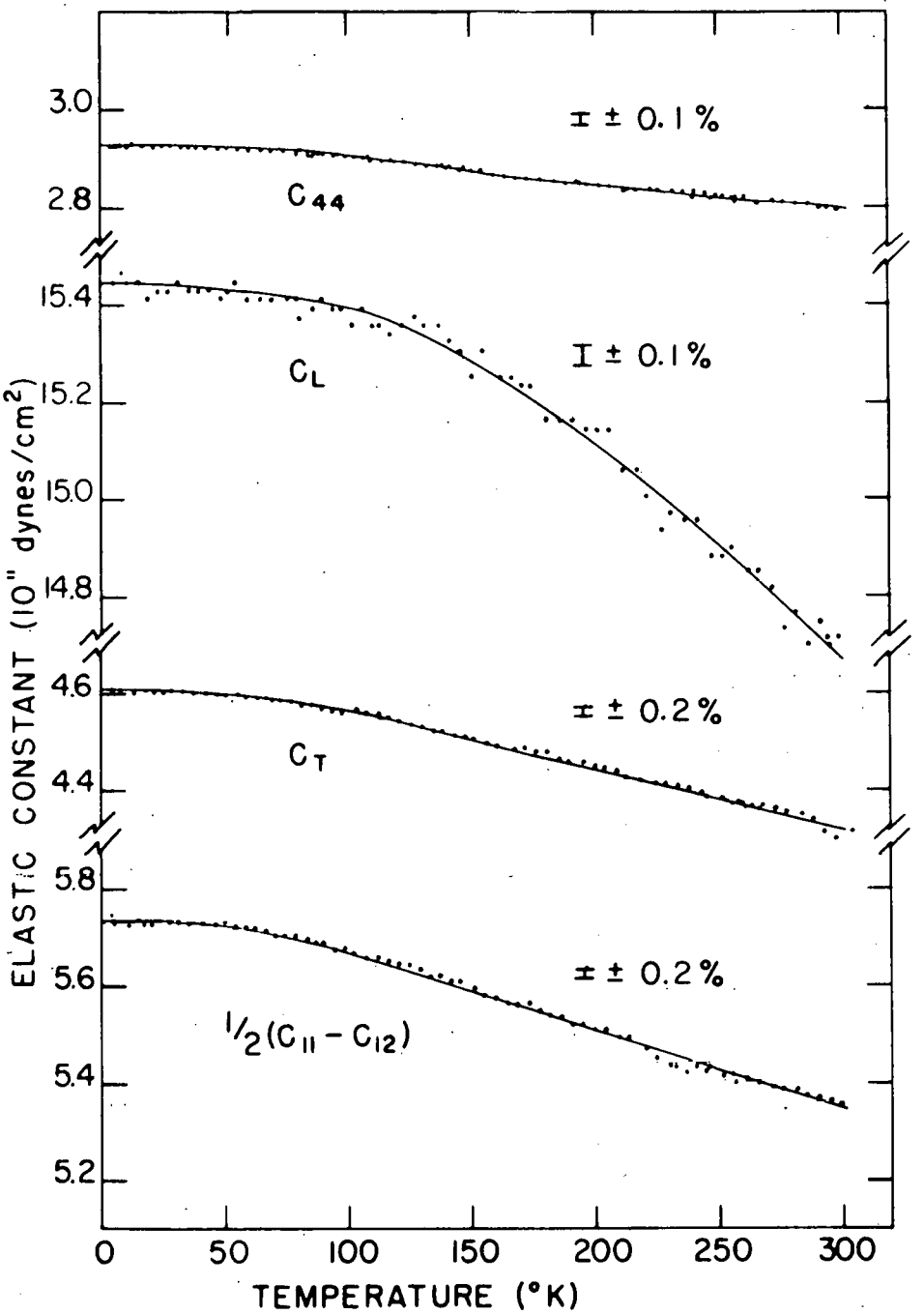

Figure 9. Single crystalline elastic constant data for Al_2Cu. C_L and C_T are associated with the quasi-longitudinal and quasi-transverse waves, respectively, propagated at 45° to [001] in (100)

Table 3. Smoothed values for the elastic constants of Zr_2Ni in 10^{11} dynes/cm^2. C_L and C_T are associated with the quasi-longitudinal and quasi-transverse waves, respectively, propagated at 45° to [001] in (100)

T(K)	C_{11}	C_{33}	C_{44}	C_{66}	C_{12}	C_{13}	$\frac{1}{2}(C_{11}-C_{12})$	C_L	C_T
4.2	15.952	14.653	2.417	0.562	13.310	7.722	1.321	13.583	3.465
10.0	15.951	14.650	2.417	0.562	13.309	7.723	1.321	13.583	3.464
20.0	15.943	14.647	2.417	0.564	13.299	7.723	1.322	13.580	3.461
30.0	15.932	14.642	2.418	0.570	13.284	7.723	1.324	13.578	3.458
40.0	15.919	14.635	2.419	0.580	13.267	7.723	1.326	13.574	3.452
50.0	15.906	14.628	2.420	0.590	13.248	7.727	1.329	13.571	3.444
60.0	15.889	14.622	2.421	0.604	13.225	7.729	1.332	13.567	3.437
70.0	15.875	14.615	2.422	0.618	13.207	7.732	1.334	13.564	3.430
80.0	15.861	14.609	2.423	0.633	13.187	7.732	1.337	13.561	3.425
90.0	15.846	14.602	2.424	0.650	13.168	7.734	1.339	13.558	3.419
100.0	15.831	14.596	2.425	0.666	13.149	7.735	1.341	13.555	3.414
110.0	15.817	14.589	2.426	0.682	13.129	7.737	1.344	13.552	3.408
120.0	15.802	14.582	2.426	0.699	13.110	7.737	1.346	13.548	3.403
130.0	15.788	14.575	2.426	0.714	13.090	7.741	1.349	13.546	3.397
140.0	15.773	14.568	2.425	0.730	13.073	7.744	1.350	13.542	3.391
150.0	15.758	14.562	2.424	0.746	13.056	7.748	1.351	13.539	3.385
160.0	15.744	14.556	2.424	0.762	13.040	7.749	1.352	13.536	3.380
170.0	15.730	14.549	2.423	0.777	13.024	7.753	1.353	13.533	3.374
180.0	15.716	14.543	2.422	0.793	13.008	7.756	1.354	13.529	3.368
190.0	15.701	14.537	2.420	0.809	12.991	7.760	1.355	13.526	3.363
200.0	15.687	14.531	2.418	0.825	12.975	7.763	1.356	13.523	3.358
210.0	15.672	14.524	2.416	0.840	12.960	7.768	1.356	13.520	3.352
220.0	15.657	14.518	2.415	0.855	12.943	7.772	1.357	13.517	3.346
230.0	15.641	14.513	2.413	0.870	12.927	7.776	1.357	13.514	3.341
240.0	15.624	14.507	2.410	0.886	12.910	7.780	1.357	13.510	3.335
250.0	15.606	14.502	2.408	0.900	12.890	7.785	1.358	13.507	3.329
260.0	15.587	14.497	2.405	0.914	12.871	7.791	1.358	13.504	3.323
270.0	15.566	14.492	2.403	0.927	12.850	7.794	1.358	13.501	3.318
280.0	15.542	14.487	2.402	0.940	12.824	7.797	1.359	13.497	3.312
290.0	15.514	14.484	2.401	0.954	12.796	7.801	1.359	13.494	3.305
300.0	15.477	14.480	2.399	0.966	12.759	7.807	1.359	13.491	3.297

Table 4. Smoothed values for the elastic constants of Al_2Cu in 10^{11}dynes/cm^2. C_L and C_T are associated with the quasi-longitudinal and quasi-transverse waves, respectively, propagated at 45° to [001] in (100)

T(K)	C_{11}	C_{33}	C_{44}	C_{66}	C_{12}	C_{13}	$\frac{1}{2}(C_{11}-C_{12})$	C_L	C_T
4.2	18.618	17.942	2.923	4.724	7.154	7.918	5.732	15.444	4.608
10.0	18.618	17.942	2.923	4.724	7.154	7.918	5.732	15.443	4.607
20.0	18.615	17.939	2.923	4.724	7.151	7.918	5.732	15.442	4.606
30.0	18.608	17.938	2.922	4.723	7.146	7.917	5.731	15.439	4.605
40.0	18.596	17.933	2.922	4.721	7.140	7.915	5.728	15.435	4.603
50.0	18.581	17.924	2.920	4.717	7.135	7.916	5.723	15.430	4.599
60.0	18.564	17.910	2.917	4.710	7.130	7.916	5.717	15.422	4.594
70.0	18.544	17.892	2.914	4.703	7.128	7.916	5.708	15.413	4.588
80.0	18.523	17.871	2.911	4.694	7.127	7.917	5.698	15.404	4.581
90.0	18.498	17.843	2.907	4.685	7.124	7.919	5.687	15.394	4.573
100.0	18.473	17.809	2.902	4.674	7.125	7.919	5.674	15.380	4.564
110.0	18.449	17.775	2.897	4.664	7.127	7.920	5.661	15.366	4.554
120.0	18.423	17.742	2.892	4.653	7.131	7.919	5.646	15.350	4.544
130.0	18.392	17.708	2.886	4.642	7.130	7.918	5.631	15.332	4.533
140.0	18.372	17.675	2.880	4.632	7.144	7.917	5.614	15.313	4.522
150.0	18.347	17.640	2.875	4.621	7.151	7.903	5.598	15.282	4.510
160.0	18.321	17.606	2.869	4.611	7.159	7.891	5.581	15.252	4.498
170.0	18.295	17.569	2.864	4.600	7.167	7.873	5.564	15.218	4.487
180.0	18.271	17.533	2.858	4.590	7.177	7.854	5.547	15.180	4.474
190.0	18.246	17.494	2.852	4.579	7.186	7.833	5.530	15.139	4.461
200.0	18.220	17.453	2.847	4.568	7.192	7.809	5.514	15.097	4.448
210.0	18.195	17.408	2.841	4.558	7.201	7.787	5.497	15.056	4.435
220.0	18.171	17.365	2.836	4.547	7.209	7.762	5.481	15.013	4.423
230.0	18.144	17.323	2.831	4.537	7.216	7.740	5.464	14.973	4.410
240.0	18.120	17.279	2.826	4.527	7.224	7.717	5.448	14.932	4.397
250.0	18.094	17.238	2.822	4.516	7.232	7.691	5.431	14.889	4.385
260.0	18.068	17.199	2.817	4.506	7.238	7.667	5.415	14.848	4.373
270.0	18.043	17.151	2.813	4.495	7.247	7.643	5.398	14.806	4.360
280.0	18.017	17.108	2.808	4.485	7.255	7.619	5.381	14.764	4.347
290.0	17.993	17.066	2.803	4.474	7.263	7.594	5.365	14.722	4.335
300.0	17.966	17.023	2.798	4.464	7.270	7.570	5.348	14.680	4.323

Greiner, Schiltz, Tonnies, Spedding, and Smith (9) resolved a similar problem for praseodymium by examining the polycrystalline moduli calculated from the single crystalline elastic constants. Their approach was applied to the present problem. Polycrystalline moduli were calculated for Al_2Cu using the Voigt-Reuss-Hill (10) average with both values for C_{13}. Table 5 gives these moduli along with the bulk moduli of elemental aluminum and copper. The bulk modulus is primarily an atomic property and one would expect the bulk modulus of a binary alloy to fall between the bulk moduli of the constituent elements. The negative value for C_{13} gave a bulk modulus for the binary alloy significantly smaller than either elemental bulk modulus while the positive value gave a bulk modulus value between the elemental bulk moduli. The positive value for C_{13} is thus more reasonable. In addition, Poisson's ratio is negative for the negative value of C_{13}. This would mean that a sample under tensile stress would show a lateral expansion. This has not been observed in metals. Since the negative value for C_{13} gave unreasonable values for both the bulk modulus and Poisson's ratio and since the positive value for C_{13} gave values that were physically reasonable, the positive value was chosen.

Attempts to grow Al_2Cu single crystals from stoichiometric alloys always produced polycrystalline samples. Since Havinga,

Table 5. Comparison of Al_2Cu polycrystalline moduli at 4.2 K calculated from single crystalline elastic constants by means of VRH average and using the two roots for C_{13}. The elemental bulk moduli of Al and Cu are included. Poisson's ratio is dimensionless and the other values are in 10^{11} dynes/cm^2

	Bulk modulus[a]	Young's modulus	Shear modulus	Poisson's ratio
$C_{13}<0$	2.39	9.36	6.17	-0.21
$C_{13}>0$	11.34	10.99	4.11	0.34
Elemental Al	7.78	-	-	-
Elemental Cu	13.71	-	-	-

[a]The bulk modulus for Al was calculated from the single crystalline elastic constant compilation of Hearmon (11) and the bulk modulus of Cu is that reported by Overton and Gaffney (12).

Damsma, and Hokkeling (13) report the phase to have a composition of $Al_{2.06}Cu$ and Hume-Rothery and Raynor (14) report $Al_{2.05}Cu$, alloys were made with approximately this composition. Single crystals from these alloys had imperfections in the form of occlusions measuring approximately 150 by 15 by 2 microns. It is believed that the presence of these occlusions can be explained on the basis of the phase diagram which is given in Figure 10. In this phase diagram, it may be noted that Al_2Cu (θ phase) appears to decompose peritectically in close proximity to the liquidus composition. The phase rule precludes the junction at a single point of the two liquidus lines, the peritectic horizontal, and the phase terminus. Thus there must be a lever arm on the aluminum-rich side at the peritectic temperature between the phase terminus and the liquidus lines. Then, to grow a single crystal, the molten alloy to be solidified must have a composition more rich in aluminum than the aluminum-rich terminus of the peritectic horizontal. In this situation, solidification of the matrix will deplete the copper concentration of the supernatent liquid and local regions will be driven to the eutectic composition and these are believed to be represented as the occluded particles. Figures 1a and 1b are photomicrographs of the (001) and (100) faces, respectively, of one of the Al_2Cu crystals. The occluded particles are oriented with their smallest dimension parallel to the [001] direction but

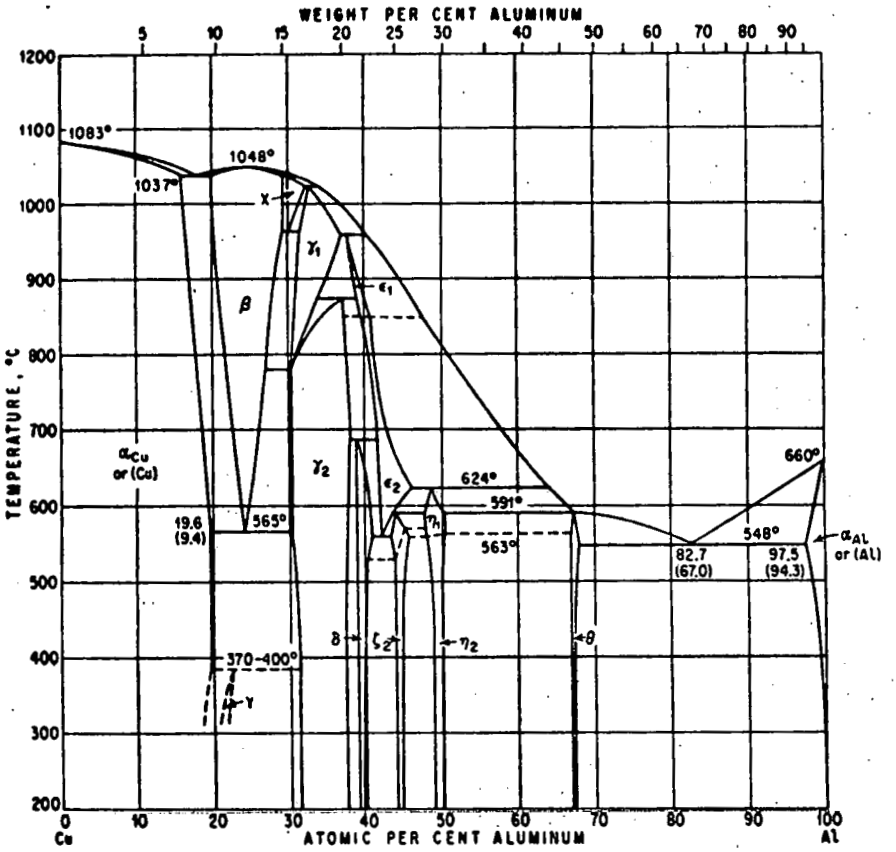

Figure 10. The aluminum-copper phase diagram as presented by Hansen (15)

show no well defined orientation of their long axis within the (001) plane.

A comparison of C_{44} data from waves propagated parallel to the [001] direction with data from waves propagated parallel to the [100] direction aids in evaluating the effect of the occluded particles on the measured values of the elastic constants. Such a comparison of raw data is given in Figure 11. In crystals of tetragonal symmetry, data from waves propagated in the [100] direction with polarization in the [001] direction should be identical to data from waves propagated in the [001] direction with polarization in the [001] direction. The 2% difference between these data illustrated in Figure 11 has been attributed to the presence of occluded particles.

Table 6 gives a further comparison of room temperature data for C_{44}. Again, waves propagated parallel to the [001]

Table 6. Comparison of room temperature C_{44} values obtained by propagating waves in the directions and with the polarizations shown

Crystal	Propagation direction	Polarization direction	C_{44} (10^{11} dynes/cm^2)
A	[001]	[100]	2.796
A	[100]	[001]	2.859
B	[110]	[001]	2.848

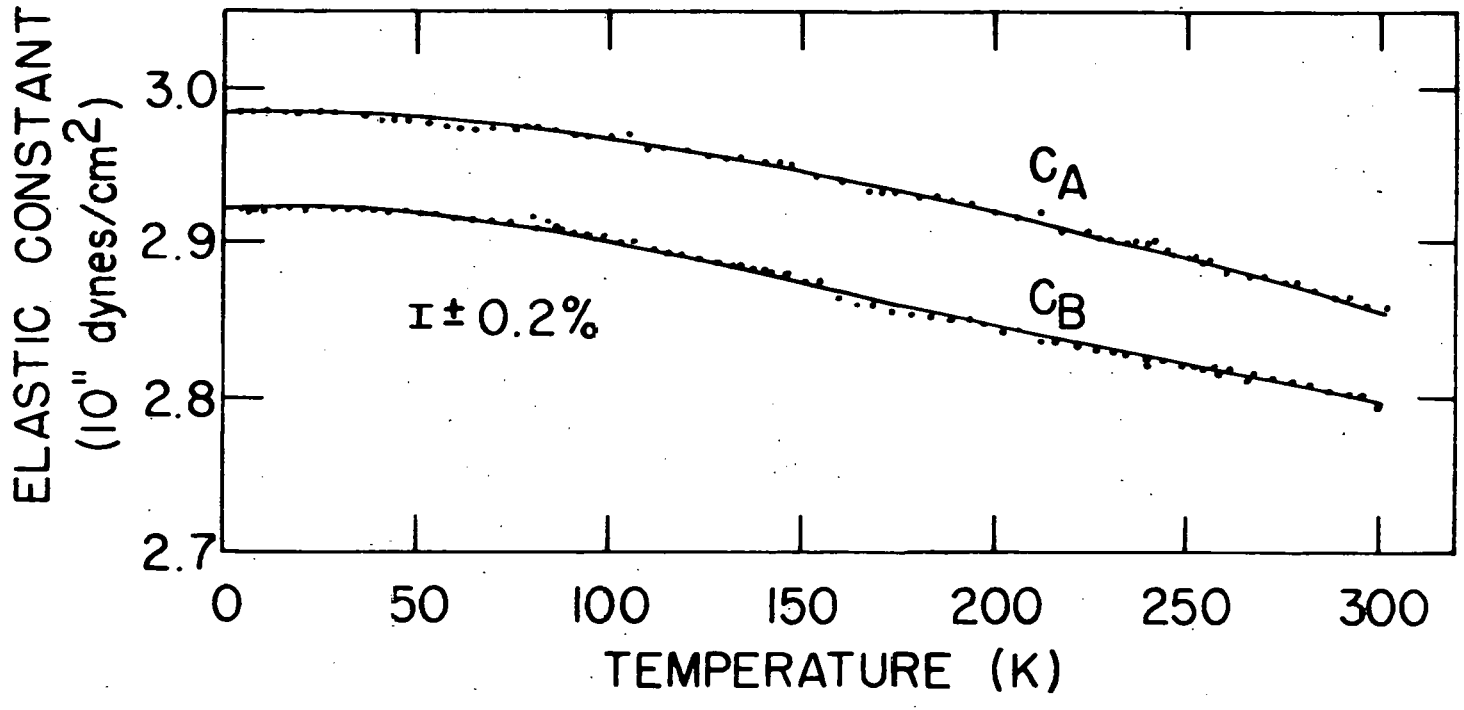

Figure 11. C_{44} data for Al_2Cu. C_A was obtained using a wave propagated in [100] and polarized in [001] and C_B was from a plane wave propagated in [001] but polarized in [100]

direction gave data about 2% greater than waves propagated parallel to the [100] direction or waves propagated parallel to the [110] direction. The good agreement of C_{44} from waves propagated parallel to the [100] and [110] directions is further indication that the occluded particles have no preferred orientation within the (001) plane.

On the basis of Goggin's (16) work on carbon-fiber in a resin matrix, it is believed that the smaller value of C_{44} is more representative of C_{44} for perfect Al_2Cu crystals. He found that elastic constant data from waves propagated normal to the fiber were much nearer the elastic constants of the matrix than were data from waves propagated parallel to the fiber. This was true for both longitudinal and shear modes.

Arguments based on the interaction of a wave and a particle concur that the smaller value of C_{44} is most representative of Al_2Cu. This follows from the fact that the interaction of a wave and a particle involves the relative size of the particles in comparison to the wavelength of the wave. The interaction is greatest when the particle size is the order of one-fourth the wavelength (17). Table 7 gives the wavelengths of the waves that were used to determine the elastic constants, their propagation directions, and the approximate projective dimensions of the occluded particles that are parallel to the wave propagation direction. All measurements were made with a pulse frequency of 10 MHz and

Table 7. The directly measured elastic constants. The propagation direction of waves that were used in determining these constants, the wavelength of the wave in microns, and the approximate dimension of the occluded particles parallel to the wave propagation direction in microns

ρV^2	Propagation direction	Wavelength	Approximate dimension of occluded particle
C_{11}	[100]	640	15 to 150
C_{33}	[001]	626	2
C_{44}	[100]	254	15 to 150
C_{44}	[001]	254	2
C_{66}	[100]	320	15 to 150
$\frac{1}{2}(C_{11}-C_{12})$	[110]	351	15 to 150
C_L	45° from [001] in (100)	581	3
C_T	45° from [001] in (100)	315	3

the differences in wavelengths are due to differences in wave velocities. The wavelengths for C_{11}, for C_{44} from a wave propagated along the [001] direction, for C_{66}, and for $1/2(C_{11}-C_{12})$ are all near the ideal size for interaction with the occluded particles and one would expect these constants to be affected most by the occluded particles. The comparison of C_{44} values given in Table 5 indicates that the error introduced by the occluded particles should not be much greater than about 2% for any of these constants. For waves that are long in comparison to the particle dimension, the sample would behave like an elastic continuum (18). Therefore, the resulting errors from the occluded particles for the other elastic constants would be much less than 2%.

DISCUSSION

Anisotropy in Zr_2Ni and Al_2Cu

In contrast to the widely accepted elastic anisotropy ratio for cubic crystals, there is no uniquely defined method for describing the elastic anisotropy of tetragonal crystals. In addition, the lower symmetry of a tetragonal crystal precludes completely describing the anisotropy by a single parameter. Vold and Glicksman (19) have chosen four factors to evaluate anisotropy in a crystal of Laue class 4/mmm. These are

$$A = C_{44}/C_{66}$$
$$B = C_{33}/C_{11}$$
$$C = C_{12}/C_{13}$$
$$D = 2C_{44}/(C_{11}-C_{12}).$$

The B factor gives an evaluation of the anisotropy related to the longitudinal elastic modes and the A and D factors are ratios of the shear modes. The C factor is related to the off diagonal stiffness constants and contains the largest inherent uncertainty. These anisotropy ratios are given for Zr_2Ni, Al_2Cu, Sn, and In in Table 8. These four are the only metallic tetragonal materials for which elastic constant data are presently available.

As Table 8 shows, the longitudinal anisotropy ratio B is near unity for all the materials listed. However, at least one shear ratio for each material is significantly different

Table 8. Anisotropy ratios and c/a ratios for Zn_2Ni, Al_2Cu, Sn, and In. Anisotropy and c/a ratios are unitless

Material	c/a[a]	A= C_{44}/C_{66}[a]	B= C_{33}/C_{11}[a]	C= C_{12}/C_{13}[a]	D= $2C_{44}/(C_{11}-C_{12})$[a]
Zr_2Ni at 4.2 K	0.812	4.303	0.919	1.724	1.830
Zr_2Ni at 300 K	0.812	2.483	0.936	1.634	1.765
Al_2Cu at 4.2 K	0.804	0.619	0.964	0.904	0.910
Al_2Cu at 300 K	0.804	0.627	0.948	0.960	0.523
Sn at 4.2 K	0.546	0.956	1.246	1.691	2.120
Sn at 300 K	0.546	0.918	1.224	1.660	3.329
In at 4.2 K	1.078	0.473	0.957	0.858	1.061
In at 300 K	1.078	0.439	0.996	0.965	2.359

[a]The c/a ratios for Sn and In were calculated from the lattice parameters listed by Cullity (20), the anisotropy ratios for Sn were calculated from the elastic constants given by Rayne and Chandrasekhar (21), and the anisotropy ratios of In were calculated from the elastic constant data of Chandrasekhar and Rayne (22).

Table 9. Superconductive transition temperatures T_c for Zr_2Ni, Al_2Cu, Sn and In

Material	T, (K)[a]
Zr_2Ni	1.58 ± 0.02
Al_2Cu	0.65 ± 0.13
Sn	3.701
In	3.408

[a]The superconductive transition temperatures of Zr_2Ni and Al_2Cu are from Havinga, Damsma, and Kanis (23) and of Sn and In are from Matthais, Geballe, and Compton (24)

from unity and one shear ratio for each material changes by 50% or more in the 4.2 to 300 K temperature range. It would be interesting to know whether other tetragonal metallic materials exhibit similar tendencies.

All four materials listed in Table 8 are superconductors and their superconductive transition temperatures are listed in Table 9. Although it is known that valence modifies the superconductive transition temperature (23,24), the data show that Al_2Cu has both the lowest anisotropy and the lowest superconductive transition temperature. Superconductivity is generally thought to arise from electron-phonon coupling and to be associated with soft phonon modes (25). Although the elastic constants give only the long wavelength limit of the phonon spectrum, a small elastic constant value and a high degree of elastic anisotropy may be taken as indicative of

soft phonon modes and hence of a tendency toward superconducting behavior.

Polycrystalline Moduli

Although it is generally not possible to calculate the exact properties of polycrystalline materials from single crystal data, approximations can be made using averaging methods. Voigt (26) proposed an approximation based on the assumption of homogeneous stress with averaging over strain. An alternate approximation was proposed by Reuss (27), who assumed homogeneous strain with averaging over stress. Because of the constraints associated with the grain boundaries in polycrystalline materials it is impossible to maintain either homogeneous stress or homogeneous strain. These methods also assume random orientation of the grains in the material, an assumption that is often violated. Hill (10) has shown that the procedures of Voigt and Reuss represent maximum and minimum values of the polycrystalline moduli and has suggested taking the mean of their approximations. This mean is often referred to as the Voigt-Reuss-Hill approximation or simply as the VRH average. The results of VRH averaging for Zr_2Ni and Al_2Cu are given in Table 10.

Smith (28) has postulated that the bulk modulus of an intermetallic phase can be approximated by the weighted mean of the bulk moduli of the constituent elements. Table 11 gives a comparison of the estimated and experimental values

Table 10. Polycrystalline moduli from VRH averaging of the single crystalline elastic constants of Zr_2Ni and Al_2Cu. The bulk modulus, K, the shear modulus, μ, and Young's modulus, E, are in units of 10^{11} dynes/cm^2. Poisson's ratio, ν, is dimensionless

	T(K)	K	μ	E	ν
Zr_2Ni	4.2	10.59	1.80	5.10	0.42
	300	10.46	1.98	5.89	0.38
Al_2Cu	4.2	11.34	4.11	10.99	0.34
	300	10.90	3.90	10.46	0.34

Table 11. Comparison of estimated and experimental room temperature bulk moduli of Zr_2Ni and Al_2Cu and their constituent elements in units of 10^{11} dynes/cm^2

A_2B	K_A[a]	K_B[a]	$\bar{K}$	K_{A_2B}	% error
Zr_2Ni	9.44	18.08	12.32	10.46	+15
Al_2Cu	7.78	13.71	9.76	10.90	-10

[a]The elemental bulk moduli of Ni and Al were calculated from single crystalline elastic constants listed in the compilation of Hearmon (11). The bulk modulus of Zr was calculated from the compressibility value given by Fisher and Renken (29) and the bulk modulus of Cu is that reported by Overton and Gaffney (12).

for Zr_2Ni and Al_2Cu. The estimated and experimental values are considered satisfactory if the discrepancy is ~10%.

The low value of the Zr_2Ni bulk modulus may be partially due to interatomic spacing. The Ni-Ni spacing in Zr_2Ni is 5.6% greater than that observed in elemental nickel. The nickel sublattice may thus be contributing less toward the bulk modulus than the atomic percentage indicates. It is also interesting to note the atomic coordination in this phase. The coordination of the nickel atoms is 10 with 2 nickel nearest neighbors and 8 zirconium nearest neighbors while the coordination number for the more abundant zirconium atoms is 15 with 4 nickel nearest neighbors and 11 zirconium nearest neighbors. The Ni-Ni interactions are thus much less numerous than the Zr-Ni or the Zr-Zr interactions.

In the case of Al_2Cu, the experimental value of the bulk modulus is 10% greater than the weighted mean moduli of the elemental constituents. Again an examination of the interatomic spacing may give a partial explanation. The bulk modulus of copper is 89% greater than the bulk modulus of pure aluminum. The interatomic distances between nearest neighbor copper atoms is 4.7% less than the interatomic spacing for elemental copper. This spacing may cause the copper sublattice to contribute more towards the bulk modulus than the atomic percentage denotes and result in a higher bulk modulus than the elemental weighted mean bulk modulus.

Debye Temperature

The Debye temperature can be calculated either from low temperature specific heat data or from the elastic constants. A linear fit of C_p/T *vs* T^2 curve is normally used to evaluate the Debye temperature from specific heat data. This method assumes only lattice and electronic contributions to the specific heat and must be made using specific heat data from near 0 K. The major difficulty in calculating the Debye temperature from elastic constant data is evaluating an integral involving the elastic constants over the solid angle. In order to overcome this problem Anderson (30) has suggested a method of deriving the Debye temperature from polycrystalline elastic moduli using an isotropic approximation. The polycrystalline moduli were calculated by the VRH averaging method that was discussed earlier. Anderson shows that his method is in good agreement with more complex procedures requiring summations over the solid angle. Anderson's method was used to determine the Debye temperature of Zr_2Ni and Al_2Cu. Table 12 gives these values along with values for the constituent elements of these alloys.

θ_o for Al_2Cu was nearly equal to the weighted mean θ_o values of the elemental constituents, while θ_o for Zr_2Ni is significantly lower than θ_o for either constituent element. This θ_o value is in keeping with the melting points. Zr_2Ni melts at 1120 C (31) and Zr and Ni melt at 1857 C and 1455 C

(32), respectively. The low θ_o for Zr_2Ni is related to the soft C_{66} and $1/2(C_{11}-C_{12})$ elastic shear modes.

Table 12. Debye temperature in degrees Kelvin for Zr_2Ni and Al_2Cu and their constituent elements. Values are from elastic constant data at 4.2 K

A_2B	$\theta_o(A)$[a]	$\theta_o(B)$[a]	$\theta_o(A_2B)$
Zr_2Ni	296	476	198
Al_2Cu	428	345	402

[a]The Debye temperatures of Ni, Al, and Cu are cited from Gschneidner (33) and of Zr is cited from Fisher and Renken (29).

REFERENCES

1. W. B. Pearson, "A Handbook of Lattice Spacings and Structures of Metals and Alloys," Pergamon Press, New York, 1958. p. 99.

2. C. Kittel, "Introduction to Solid State Physics," Fourth Edition, John Wiley and Sons, Inc., New York, N.Y., 1971. pp. 135-147.

3. R. E. Hungsberg and K. A. Gschneidner, Jr., J. Phys. Chem. Solids 33, 401 (1972).

4. R. W. Meyerhoff, D. M. Bailey, and J. F. Smith, Rev. Sci. Instrum. 32, 715-717 (1961).

5. J. E. May, Jr., IRE Natl. Conv. Rev. 6, Pt. 2, 134 (1958).

6. E. P. Papadakis, J. Acoust. Soc. Amer. 42, 1045 (1967).

7. D. H. Chung, D. J. Silversmith, and B. B. Chick, Rev. Sci. Instrum. 40, 718 (1969).

8. G. A. Alers and J. R. Neighbours, J. Appl. Phys. 28, 1514 (1957).

9. J. D. Greiner, R. J. Schiltz, Jr., J. J. Tonnies, F. H. Spedding, and J. F. Smith, J. Appl. Phys. 44, 3862-3867 (1973).

10. R. Hill, Proc. Phys. Soc. (London) A65, 349 (1952).

11. R. F. S. Hearmon, in "Landolt-Bornstein Tables," Vol. 2, K. H. Hellwege, Ed., Springer-Verlag, New York, 1969. pp. 1-39.

12. W. C. Overton, Jr., and John Gaffney, Phys. Rev. 98, 969-977 (1955).

13. E. E. Havinga, H. Damsma, and P. Hokkeling, J. Less-Common Metals 27, 169-186 (1972).

14. W. Hume-Rothery and G. V. Raynor, "The Structure of Metals and Alloys," The Institute of Metals, London, 1926. p. 176.

15. M. Hansen, "Constitution of Binary Alloys," McGraw-Hill Book Company, Inc., New York, 1958. p. 85.

16. P. R. Goggin, J. Mat. Sci. 8, 233-244 (1973).

17. W. Shockley, "Electrons and Holes in Semiconductors," D. Van Nostrand Company, Inc., New York, 1950. p. 265.

18. V. K. Tewary and R. Bullough, in "Treatise on Materials Science and Technology," Vol. 1, H. Herman, Ed., Academic Press, New York, 1972. pp. 115-118.

19. C. L. Vold and M. E. Glicksman, Rept. NRL. Prog., February 1972, pp. 27-28.

20. B. D. Cullity, "Elements of X-Ray Diffraction," Addison-Wesley Publishing Company, Inc., 1956. pp. 482-484.

21. J. A. Rayne and B. S. Chandrasekhar, Phys. Rev. 120, 1658-1663 (1960).

22. B. S. Chandrasekhar and J. A. Rayne, Phys. Rev. 124, 1011-1014 (1961).

23. E. E. Havinga, H. Damsma, and J. M. Kanis, J. Less-Common Metals 27, 281-291 (1972).

24. B. T. Matthias, T. H. Geballe, and V. B. Compton, Rev. Mod. Phys. 35, 1-22 (1963).

25. I. M. Firth, "Superconductivity," Mills & Boon Limited, 1972. p. 41.

26. W. Voigt, "Lehrbuch der Kristalphysik," Teubner, Leipzig, 1928. pp. 716-761.

27. A. Reuss, Z. Angew. Math. Mech. 9, 55 (1929).

28. J. F. Smith, in "Nuclear Metallurgy," Vol. 10, J. T. Waber, P. Chiotti, and W. N. Miner, Ed., Edwards Bros., Ann Arbor, Mich., 1964. p. 397.

29. E. S. Fisher and C. J. Renken, Phys. Rev. 135, A482-A494 (1964).

30. O. L. Anderson, J. Phys. Chem. Solids 24, 909-917 (1963).

31. M. E. Kirkpatrick and W. L. Larsen, Trans. Amer. Soc. Metals 54, 580 (1961).

32. C. D. Hodgman, Ed., "Handbook of Chemistry and Physics," Chemical Rubber Publishing Co., Cleveland, Ohio, 1958. pp. 405-436.

33. K. A. Gschneidner, Jr., Solid State Physics 16, 275-426 (1964).

ACKNOWLEDGMENTS

First, I want to acknowledge my family. Without the affection, prayer, financial support, and encouragement of my wife, Marcene, this project would have been impossible. I want to thank her deeply and say that our marriage is much more meaningful now than when we started this task together. Paul, Steve, Mark, and John, my sons, have continued to give their moral support. In addition, Steve and Mark helped directly in the collection of data and preparation of samples.

I have learned much under the leadership of Dr. J. F. Smith, my major professor. His willingness to spend several evenings correcting this manuscript is particularly appreciated.

The expertise and encouragement of many other staff, students, and friends have made this project easier and more fruitful. I am sincerely grateful for their help.